Oriented, Active *Escherichia coli* RNA Polymerase: An Atomic Force Microscope Study

Neil H. Thomson,* Bettye L. Smith,*# Nils Almqvist,* Lutz Schmitt,§ Mikhail Kashlev,¶ Eric T. Kool,‖ and Paul K. Hansma

*Department of Physics and #Materials Research Laboratory, University of California Santa Barbara, Santa Barbara, California 93106; §Department of Chemistry, Stanford University, Stanford, California 94304-5080; ¶National Cancer Institute, Frederick Cancer Research and Development Center, Frederick, Maryland 21702-1201; and ‖Department of Chemistry, University of Rochester, Rochester, New York 14627 USA

ABSTRACT Combining a system for binding proteins to surfaces (Sigal, G. B., C. Bamdad, A. Barberis, J. Strominger, and G. M. Whitesides. 1996. *Anal. Chem.* 68:490–497) with a method for making ultraflat gold surfaces (Hegner, M., P. Wagner, and G. Semenza. 1993. *Surface Sci.* 291:39–46 1993) has enabled single, oriented, active *Escherichia coli* RNA polymerase (RNAP) molecules to be imaged under aqueous buffer using tapping-mode atomic force microscopy (AFM). Recombinant RNAP molecules containing histidine tags (hisRNAP) on the C-terminus were specifically immobilized on ultraflat gold via a mixed monolayer of two different ω-functionalized alkanethiols. One alkanethiol was terminated in an ethylene-glycol (EG) group, which resists protein adsorption, and the other was terminated in an N-nitrilotriacetic acid (NTA) group, which binds the histidine tag through two coordination sites with a nickel ion. AFM images showed that these two alkanethiols phase-segregate. Specific binding of the hisRNAP molecules was followed in situ by injecting proteins directly into the AFM fluid cell. The activity of the hisRNAP bound to the NTA groups was confirmed with a 42-base circular single-stranded DNA template (rolling circle), which the RNAP uses to produce huge RNA transcripts. These transcripts were imaged in air after the samples were rinsed and dried, since RNA also has low affinity for the EG-thiol and cannot be imaged under the buffers we used.

INTRODUCTION

Applications of atomic force microscopy (AFM) (Binnig et al., 1986) in biology increasingly involve studying dynamic biological processes (Kasas et al., 1997; Radmacher et al., 1994; Thomson et al., 1994, 1996) and detecting molecular forces (Florin et al., 1994; Lee et al., 1994a, b; Moy et al., 1994). For measuring interaction forces between molecules, developments in the measurement of cantilever spring constants (Cleveland et al., 1993) and methods for anchoring molecules to tips and surfaces have enabled single molecule interactions to be resolved (Florin et al., 1994; Lee et al., 1994b; Moy et al., 1994). For studying processes, the invention of AC imaging modes (Dreier et al., 1994) such as fluid tapping mode (Hansma et al., 1994; Putman et al., 1994) has been crucial in preventing damage and distortion of the systems during imaging (Fritz et al., 1995; Kasas et al., 1997; Thomson et al., 1996a, b). Both applications would benefit greatly if the orientation of the molecules on the surface were controlled. For molecular force detection, orienting the molecules with the active site accessible prevents topological constraints from hampering data acquisition and interpretation. Orienting proteins with their active sites away from the surface is also extremely important for measurements of the activity and motion of enzymes (Kasas et al., 1997; Radmacher et al., 1994). With proper orientation, the percentage activity of an enzyme on a surface should go up, thus increasing the likelihood of observing events related to activity by AFM (a point probe technique). If the orientation of the enzyme is known, then it may also be possible to relate observation of conformational changes to the structure of the enzyme.

Mica has been the popular choice for supporting proteins to be imaged by AFM. Success in imaging relies on the fact that the protein-mica interaction is stronger than the tip-protein interaction. Proteins in this case are physisorbed to the mica, electrostatic forces being dominant. Many proteins will not spontaneously physisorb to mica under the buffer conditions that are most suitable for their activity in vitro. Methods of attaching proteins to surfaces are desirable when undertaking experiments to gain new insight into protein structure and function with the AFM, as mentioned above. Previous work has predominantly utilized self-assembled monolayers (SAMs) on gold for immobilizing proteins for AFM imaging (Delamarche et al., 1996; Patel et al., 1997; Wagner et al., 1994, 1996). These studies have not concentrated on specific orientation of molecules, since the reaction with the support surface is through amine or –CH groups on the proteins. Another study claims to have oriented antibodies through thiol groups on gold surfaces (Droz et al., 1996)

We present a new general method for orienting histidine-tagged proteins on functionalized gold surfaces that are flat enough for unambiguous imaging of the proteins by AFM.

Received for publication 10 October 1997 and in final form 23 October 1998.

Address reprint requests to Bettye L. Smith, Department of Physics, University of California, Santa Barbara, CA 93106. Tel.: 805-893-3999; Fax: 805-893-8315; E-mail: bettye@mrl.ucsb.edu.

Nils Almqvist's permanent address is Department of Physics, Luleå University of Technology, S-97187 Luleå, Sweden.

0006-3495/99/02/1024/10 $2.00

The anchoring involves the chelation of two histidine residues in the tag (usually six histidines long) with a nickel ion bound by four other sites to an N-nitrilotriacetic acid (NTA) group (Hochuli et al., 1987) which is situated on the end of an alkanethiol molecule. Alkanethiols readily form self-assembled monolayers on gold surfaces (Dubois and Nuzzo, 1992; Whitesides and Gorman, 1995). By mixing the NTA thiol with one terminated with an ethylene-glycol (EG) group, which resists protein adsorption, it has been possible to specifically bind and distinguish single protein molecules with the AFM. The advantages of this two-thiol system for orienting proteins has been described previously (Sigal et al., 1996). These include (i) keeping the active site away from the surface through specific binding at one site; (ii) immobilizing histidine-tagged proteins while resisting nonspecific adsorption of others; and (iii) avoiding modifications of the protein through nonspecific covalent binding. For AFM purposes, the thiols on gold are attractive because extremely flat functional surfaces can be made relatively easily.

The protein used in this study was a recombinant *Escherichia coli* RNA polymerase (RNAP), a large (480 kDa) multidomain enzyme responsible for converting the genetic information encoded in DNA into complementary sequences of messenger RNA in the process known as transcription. The histidine tag was genetically added to the C-terminus of the β'-subunit of the RNAP and has been shown to maintain activity when bound to NTA agarose beads (Kashlev et al., 1993). The activity of the histidine-tagged RNAP (hisRNAP) on the functionalized gold was assessed by complexing it with a 42-base circular single-stranded DNA, known as a rolling circle (Rubin et al., 1995). These rolling circle templates produce huge RNA transcripts (between 400 and 9000 bases long; Daubendiek et al., 1995) that can be distinguished after drying the sample and imaging using tapping mode in air (Kasas et al., 1997) .

MATERIALS AND METHODS

Gold surfaces

Ultra-flat gold surfaces were made using a slightly modified version of Hegner's template-stripping method (Hegner et al., 1993). Gold was deposited onto freshly cleaved mica surfaces and these were then glued, gold-side down, using a very low viscosity two-component thermally curable epoxy (epo-tek 377, Epoxy Technology Inc., Billerica, MA), onto steel disks, which are used for mounting on the AFM tube scanner. The mica can be stripped, chemically and/or mechanically, to reveal the gold surface that mimics the atomically flat mica surface. The morphology of the stripped gold surface depends on the method of deposition (evaporation or sputtering), the mica temperature during deposition, the vacuum pressure, and the deposition rate. Gold surfaces with suitable morphologies for distinguishing RNA polymerase by AFM were achieved using three different protocols: (i) sputtering gold onto mica heated to ~300°C at 50 millitorr in an argon environment; (ii) evaporating gold onto mica at room temperature in a vacuum below 2×10^{-6} torr with a deposition rate of ~0.13 nm/s; and (iii) evaporating gold onto mica heated to ~350°C in a vacuum of between 5×10^{-6} and 7×10^{-6} torr with a deposition rate of ~15 nm/s (see Fig. 1). The gold films were deposited to thicknesses of 150–200 nm to ensure mechanical stability during subsequent manipulation. The mica was stripped from these gold surfaces using a combination of chemical treatment and mechanical means. The sandwiches of steel, glue, gold, and mica were wholly immersed in tetrahydrofuran (THF) until the mica was loose enough to be cleaved from the gold surface in one motion using a razor blade. The amount of time that the steel-glue-gold-mica sandwiches required in THF varied depending upon the deposition method, though there was also significant variation within the same batch. In general, longer incubation times in THF were required for the flatter gold surfaces. This can be explained with the hypothesis that a flatter gold surface provides greater adhesion between the mica and gold. Examples of AFM images of the three types of gold surfaces are shown in Fig. 1. In these instances, incubation times in THF were 3 h for the sputtered gold [method (i); Fig. 1 *a*], 2 h for the slowly evaporated gold [method (ii); Fig. 1 *b*], and 1 h for the fast-evaporated gold [method (iii); Fig. 1 *c*].

Synthesis of alkanethiols

The two functionalized alkanethiols, thioalkyl-triethyleneglycol (EG-thiol) and thioalkyl-triethyleneglycol-nitrilotriacetic acid (NTA-thiol) were synthesized according to the methods of the Whitesides group (Pale-Grosdemange et al., 1991; Sigal et al., 1996). All intermediates and the final products were characterized by TLC, NMR, and mass spectroscopy.

Thiol SAMs

The self-assembled monolayers (SAMs) of ω-functionalized alkanethiols were formed on the freshly stripped gold surfaces by incubating the surfaces in 1 mM ethanolic solutions (HPLC grade) of the thiols between 18 and 24 h. The percentage concentrations of the two components, nitriloacetic acid (NTA) and ethylene-glycol (EG), were varied to investigate monolayer formation (see Fig. 2), though the overall thiol concentration was kept at 1 mM. On removal from the ethanol/thiol solutions, the gold surfaces were rinsed in excess ethanol and dried in a stream of argon gas and stored in a desiccator until required for use in the AFM experiments. In principle, these surfaces should last indefinitely under these conditions, although in practice we found that the surfaces degraded or were contaminated over a six-month period, probably due to periodic opening of the desiccator.

Preparation of oriented RNA polymerase samples

To attach the histidine-tagged *E. coli* RNA polymerase (hisRNAP) specifically to the SAMs, the surfaces were first incubated in 1 mM NaOH for 5 min and then in 40 mM $NiSO_4$/1 mM NaOH for 1 h at room temperature. This is necessary since the binding of nickel to the NTA group is strongest in alkaline pH. The surface was then rinsed with a transcription buffer compatible with maintaining the activity of RNAP (20 mM Tris pH 7.9, 5 mM $MgCl_2$, 50 mM KCl, 1 mM β-mercaptoethanol) and introduced into the microscope under the same buffer.

Two types of experiments were performed with the AFM; the protein was either added to the surfaces outside the microscope (see preparation of rolling circle complexes), or injected into the fluid cell during imaging to monitor binding to the surface. In the experiments to determine activity with the rolling circle, the hisRNAP was added outside the microscope. These surfaces were thoroughly rinsed with the transcription buffer before mounting in the microscope to remove weakly bound hisRNAP or unbound hisRNAP. The activity assays were carried out under continuously flowing buffer, ensuring that only surface-bound hisRNAP was present.

Preparation of the rolling circle complexes

One mM of a 42-base circular single-stranded DNA (known as a rolling circle; Daubendiek et al., 1995) was incubated with 0.4 mM of hisRNAP at 37°C for 10 min. A ribonucleoside triphosphate (NTP) mixture (ATP,

CTP, UTP, GTP) was added to the reaction at a final concentration of 2.5 μM for each NTP. In this low concentration of NTPs the hisRNAP will only form a transcript of 10 to 20 bases in length (Kasas et al., 1997). The complex was diluted and added to the solution on the gold, incubated for ~10 min at room temperature, and then rinsed with excess buffer.

Atomic force microscopy

The atomic force microscope was a Digital Instruments Nanoscope III (Santa Barbara, CA) used with a D scanner (maximal scan range of ~12 μm). We used a Plexiglas fluid cell and all imaging was carried out using tapping mode. For tapping in fluids we used 100-μm-long silicon nitride cantilevers with nominal spring constants of 0.10 N/m, with electron-beam deposited tips (Akama et al., 1990; Keller and Chih-Chung, 1992). For imaging in air we used 125-μm diving board silicon levers with nominal spring constants of 30 N/m. The cantilevers were driven close to their resonant frequencies, ~9–13 kHz in the aqueous buffers and ~250 kHz for the levers in air. Image acquisition times were between 30 and 90 s for images with pixel resolutions of 256 × 256. The images were flattened, off-line, using zero- or first-order polynomial fits to account for Z offsets and sample tilt (Nanoscope Software, Digital Instruments).

Extremely small volumes (10 μl or less) of hisRNAP solutions were injected into the fluid cell (without O-ring) using fine ceramic needles (World Precision Instruments, Sarasota, FL) and glass syringes (Hamilton Co., Reno, NV). The flexible needles were inserted into a larger syringe needle glued to the underside of the fluid cell module to enable delivery of small volumes of solution directly into the middle of the fluid cell close to the tip during imaging. The syringe needle was positioned to guide the ceramic needle to the correct place so that the imaging was not significantly perturbed during injection.

The activity of hisRNAP was determined by AFM as previously described (Kasas et al., 1997). Briefly, to assay the activity of the hisRNAP on these functionalized surfaces, the rolling circle complexes were imaged under continuously flowing transcription buffer (see above). The transcription buffer containing 5 mM NTPs was then flowed through the fluid cell for 10–20 min. These samples were then removed from the microscope, rinsed in excess water, dried, and imaged tapping-mode in air.

RESULTS

The three suitable types of gold surfaces we made for distinguishing proteins in the AFM are shown in Fig. 1. Previously, much work has been carried out to make very flat evaporated gold films on mica (Chidsey et al., 1988; Manne et al., 1990; Putnam et al., 1989; Vancea et al., 1989). To make gold films on mica that are suitable for biological samples studied by AFM the substrate temperature and evaporation conditions must be rigorously controlled. The replication technique of Hegner et al. (1993) has the advantage that the surfaces can be kept indefinitely as a "sandwich" and the gold exposed only when required. We extended Hegner's method to include sputtering as a deposition technique. The RMS roughnesses of the surfaces were smallest when the mica was heated (see Fig. 1 caption). We found that making the flattest gold possible was not always best for our purposes, since it was more difficult to remove the mica, as indicated by the residual mica flakes on the sputtered gold surface (see *arrow*, Fig. 1 *a*). Having the smallest possible RMS roughness is not always the most important factor for biological AFM. For example, sputtered gold on mica made at room temperature produced surfaces with low RMS roughness (between 0.3 and 0.5 nm over 25-μm^2 areas) but had a grain size of ~30 nm, which is about the same size that RNAP appears in the AFM. The evaporated films were generally rougher but had larger grains with flat plateaus on top, on which the RNAP molecules were easily distinguishable. It should be noted that the top surfaces of the gold films were always rougher than the mica-stripped surfaces, and unsuitable for our purposes. We found that the gold surfaces made by the fast, hot

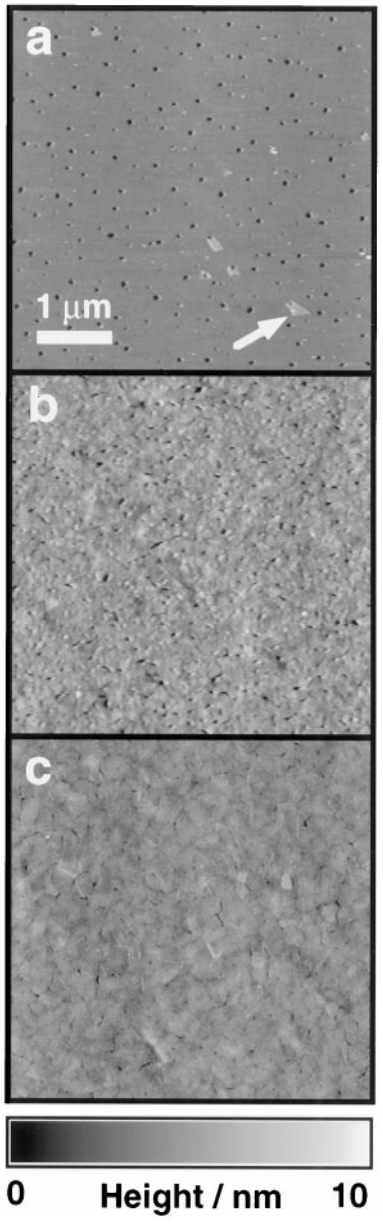

FIGURE 1 Ultraflat gold surfaces stripped from mica surfaces imaged using tapping mode in air. They were prepared using three different deposition methods: (*a*) gold sputtered onto mica heated to ~300°C in an argon atmosphere at 50 millitorr, (*b*) gold evaporated onto mica at room temperature with a deposition rate of 0.13 nm/s and pressure below 2 × 10^{-6} torr, and (*c*) gold evaporated onto mica heated to ~350°C with a deposition rate of ~15 nm/s at a pressure between 5 × 10^{-6} and 7 × 10^{-6} torr. Typical RMS roughness of these surfaces over areas of 25 μm^2 are 0.28 nm, 0.54 nm, and 0.33 nm.

evaporation method (see Fig. 1 *c*) were the most convenient when comparing flatness with ease of stripping the mica.

Fig. 2 shows gold surfaces made using the fast, hot evaporation method (see Fig. 1 *c*) incubated in two different percentages of NTA-thiol. With no NTA thiol (Fig. 2 *a*), we observed some contaminant particles that adsorbed predominantly to the grain boundaries. With increasing percentage of NTA-thiol, up to 10%, we observed features that were 1–3-nm higher than the rest of the surface (see Fig. 2 *d*) that occurred all across the surface, and not only at the grain boundaries (see Fig. 2 *b*). Specifically, there are 35 features in Fig. 2 *b* protruding from the surface. Of these 35, 12 are next to holes; of these 12, 8 have the characteristic appearance of contaminants present in Fig. 2 *a*. This indicates that there are 23 features that can be attributed to the presence of NTA. We attribute these "islands" to phase segregation of the NTA-thiol from the EG-thiol into domains below 100 nm in their maximum lateral dimensions. Previous ellipsometry measurements could not determine whether the NTA-thiol was phase-segregated or homogenously mixed with the EG-thiol (Sigal et al., 1996). Fig. 2 *c* shows that the NTA-thiol forms elongated "islands" and the protrusion of the NTA-thiol above the surface is consistent with a bulkier headgroup than the EG-thiol (see Fig. 2 *d*). The coverage of the "islands" at 3, 5, and 10% NTA was measured and found to be consistent with increasing percentage of NTA-thiol in the incubating ethanolic solution. At very high concentrations of NTA-thiol (>95%), the thiols do not seem to form a monolayer (data not shown), presumably because the bulky NTA headgroup hinders the alkyl chain interaction that stabilizes monolayer formation. NTA percentages between 10 and 95% were not investigated.

To study the binding of the histidine-tagged RNAP (hisRNAP) to these surfaces, we needed to know up to which protein concentration the EG-thiol was resistant to adsorption. We used fine ceramic needles and 10-μl glass syringes to inject hisRNAP solutions directly into the fluid cell close to the imaging tip. This method was chosen because the hisRNAP was in limited supply and there is a large dead volume (~0.6 ml) in the injection port to the fluid cell. It

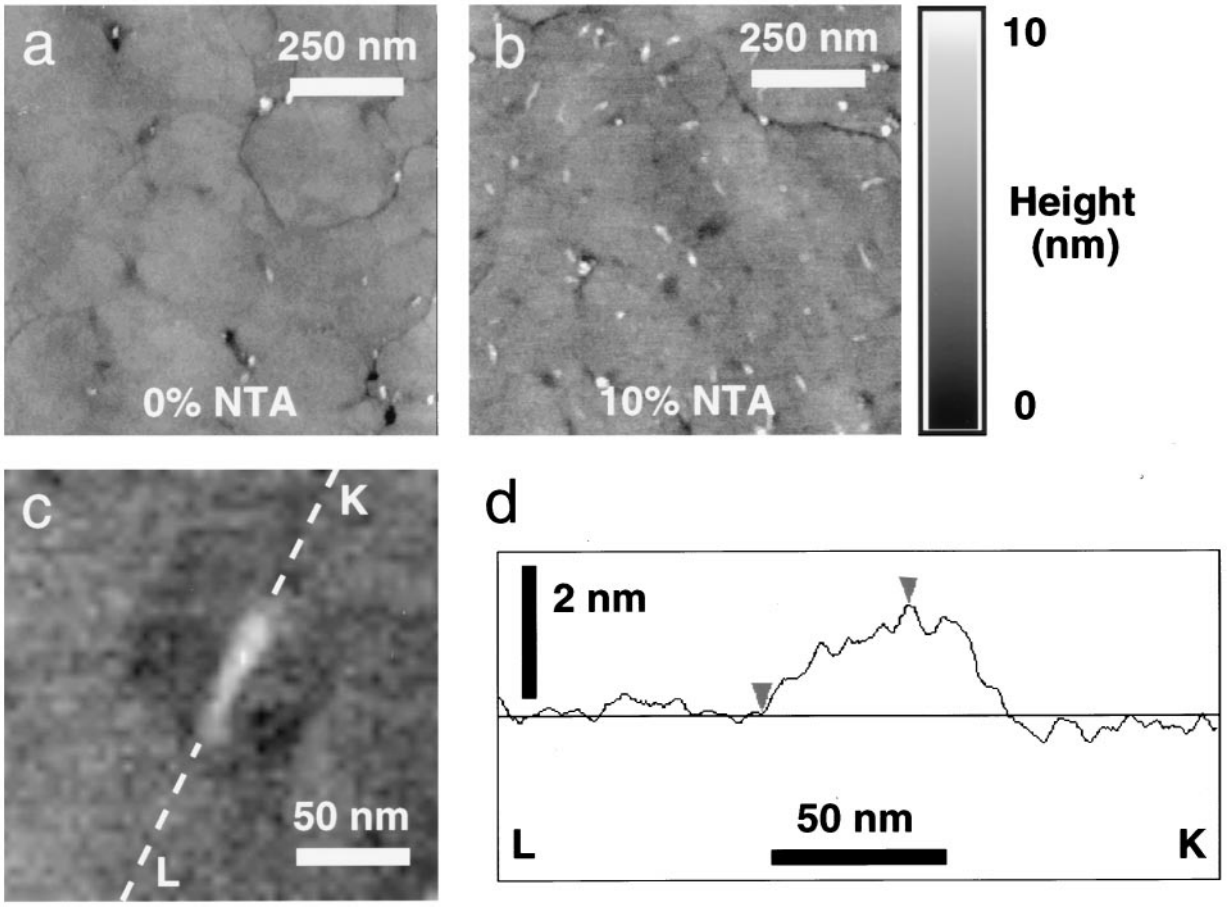

FIGURE 2 Gold surfaces covered with (*a*) a pure monolayer of EG-thiol, with no NTA-thiol present, and (*b*) a mixed monolayer formed from incubation in 90% EG-thiol and 10% NTA-thiol. The gold surfaces were prepared using the fast, hot evaporation method (see Fig. 1 *c* and Materials and Methods). With no NTA present there are some contaminant particles of unknown origin bound to the grain boundaries (*a*). With 10% NTA-thiol we observed phase separation from the EG-thiol into "islands" that are distributed over the whole gold surface (*b*). These are long and thin in appearance and protrude 1–3 nm higher in the images than the surrounding EG-thiol because of the extra bulky NTA headgroup. (*c*) A software zoom of one of the "islands" in (*b*); (*d*) a line-profile through this "island" along the line LK. The height difference between the two markers is 1.66 nm. Images were acquired using tapping mode under water.

was difficult to exactly quantify the final protein concentration since the volume of the fluid in the cell was not well defined (because of the lack of an O-ring). Also, the amount of protein solution injected was not easy to control and varied between ~1 and 5 μl. We estimate the amount of hisRNAP injected into the fluid cell by assuming injection of 1 μl of solution. A good estimate for the volume of the fluid cell is ~50 μl with no O-ring. The exact concentration of hisRNAP at any point on the surface is difficult to assess because there will be a concentration gradient from the point of injection. Fig. 3 shows four images of gold surfaces covered with 100% EG-thiol, taken after different amounts of hisRNAP were injected into the microscope fluid cell. With no hisRNAP present there were small contaminant particles bound to the edges of the gold plateaus (Fig. 3 *a*). After injection of ~5 ng of hisRNAP the surface shows no adsorption of protein in the same scan area (Fig. 3 *b*). In a new scan area (Fig. 3 *c*), as the amount of hisRNAP injected was increased to ~24 ng, protein molecules were observed bound to the grain boundaries. In the same scan area (Fig. 3 *d*), ~240 ng of RNAP was injected and more protein molecules were observed bound to the grain boundaries (*arrow*). At the highest amount of protein injected we never observed binding to the middle of the plateaus. The hisRNAP molecules bind to the edges of the plateaus possibly because the coverage of the EG-thiol is less uniform. For all subsequent experiments we injected <5 ng or used a protein concentration of <0.1 μg/ml of hisRNAP to avoid unspecific adsorption.

Specific binding of the hisRNAP to the NTA islands was observed by injecting ~2 ng of hisRNAP into the fluid cell during scanning. Fig. 4 *a* shows six sequential images of hisRNAP molecules binding to the NTA islands, three of which are indicated by arrows in image one. Single hisRNAP molecules bind to these three islands during this sequence. Times in minutes and seconds are shown in each image. One hisRNAP binds very soon after injection in image one. The first image in this sequence is the first image acquired after injection; another hisRNAP binds two images later (image 3) and then two more bind in image 5, though one of

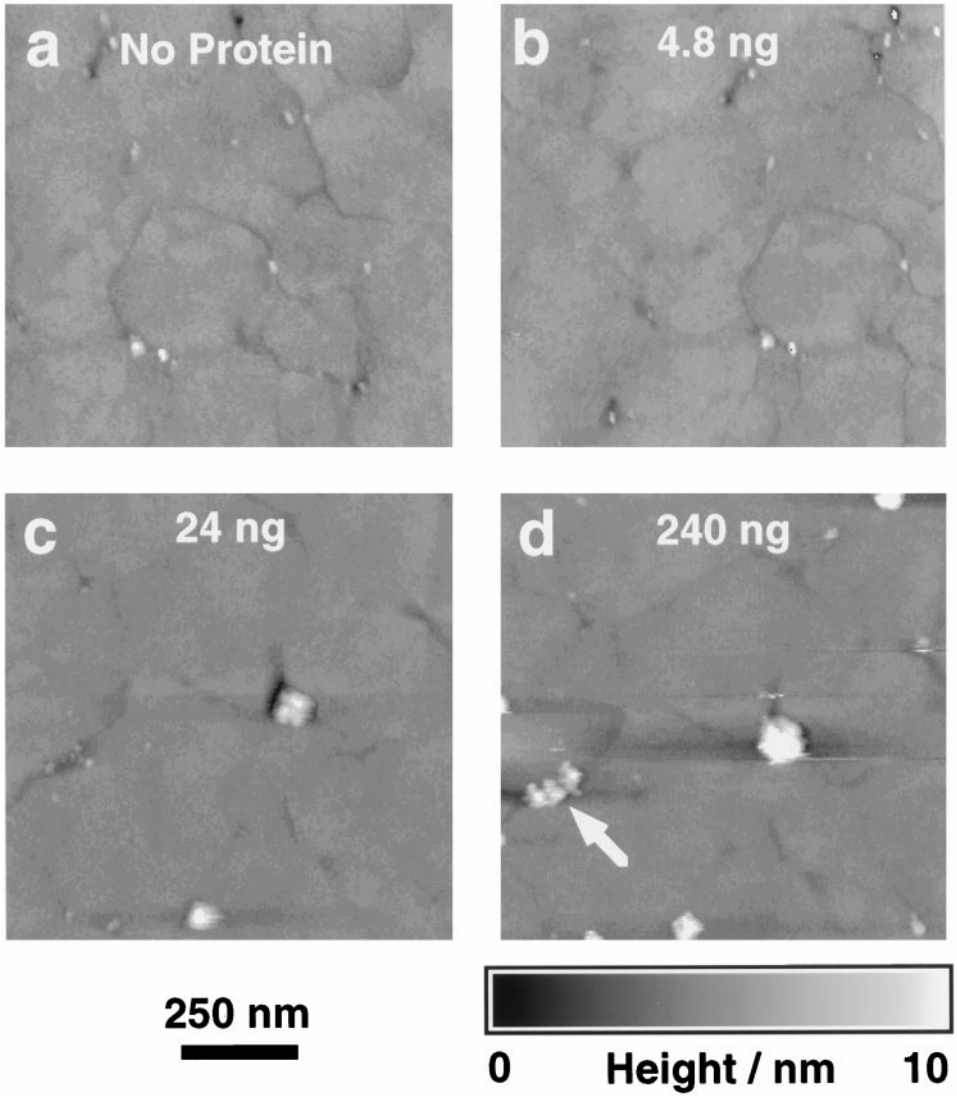

FIGURE 3 Unspecific binding of hisRNAP to gold surfaces terminated with just the EG-thiol (0% NTA thiol) was tested by injecting various amounts of hisRNAP into the microscope fluid cell and observing adsorption behavior. The approximate amount of hisRNAP in the fluid cell is shown at the top of each image. In (*a*) some contaminant particles are bound to the grain boundaries. After injection of ~5 ng of protein no adsorption was observed in the same scan area (*b*). The area scanned in (*b*) is offset slightly relative to (*a*) because of drift. In a new scan area (*c*), after injection of 24 ng of protein, unspecific binding of protein molecules occurred at the grain boundaries. After injection of 240 ng of hisRNAP (*d*), the same scan area as (*c*) shows more protein molecules binding to the grain boundaries (*arrow*). These images were acquired using tapping mode under the transcription buffer. All experiments involving specific binding of hisRNAP were carried out by injecting <5 ng of hisRNAP.

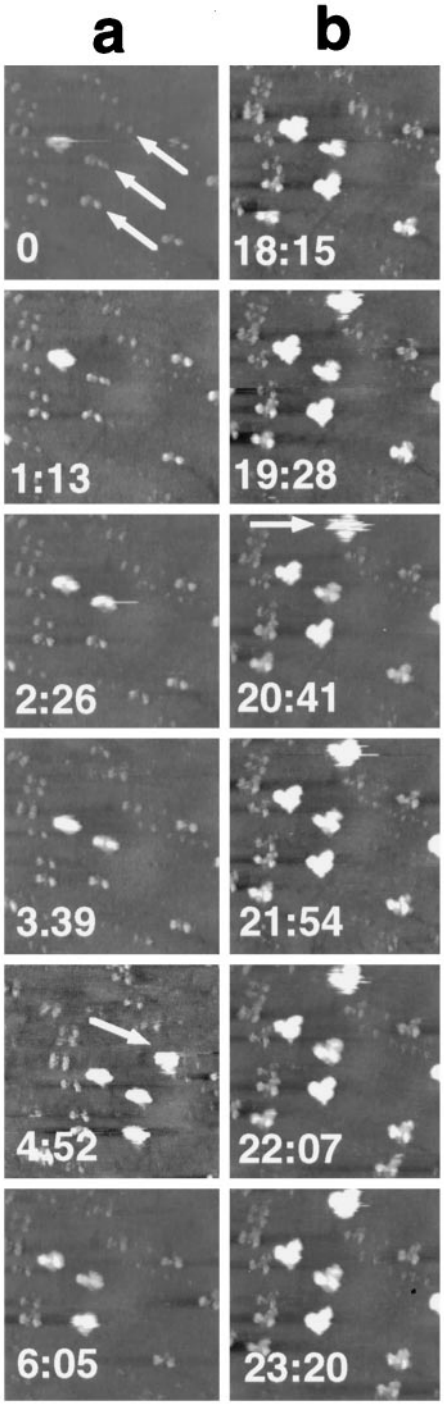

FIGURE 4 (*a*) Six sequential images of the same area showing single hisRNAP molecules binding to the nickel-NTA islands. The image acquisition time was ~73 s; the time in minutes and seconds is shown in each image. Most molecules bind on a much faster time scale than the images take to acquire. One hisRNAP is bound in image 5 but was unbound before image 6 was acquired (see *arrow* in image 5). Note that a double tip developed during imaging. (*b*) Six sequential images taken from the same experiment as (*a*), 12 min and 10 s after the last image in (*a*) was acquired. The hisRNAP binding in the top of these images illustrates that some hisRNAP take a few images before they bind stably to the NTA groups (see *arrow* in image 3). Note that the tip shape has changed to a triple tip. These sequences were acquired using tapping mode under the transcription buffer. Each image is 600 nm × 600 nm.

these unbinds before the sixth image is acquired (see arrow in image 5). Each image took 73 s to acquire, so it is clear that these binding events occurred well below this time scale. However, cases were observed where proteins took several frames to bind firmly to the surface (see Fig. 4 *b*). The hisRNAP at the top of these images is moving around underneath the tip for a few images before it settles (see arrow in image 3). Fig. 4 illustrates a problem sometimes encountered when observing dynamic biological events with the AFM. The tip at the beginning of the experiment has a twinned appearance (Fig. 4 *a*) and changes during the experiment to a triple tip (Fig. 4 *b*). The tip shape can change while imaging due to contaminants (e.g., proteins) binding to the tip. Fig. 5 shows a representative image of a sample prepared ex situ. In these cases contamination to the tip did not occur and individual RNAP molecules are clearly imaged.

Nonspecific binding of the hisRNAP could occur to the NTA islands if the concentration of protein was too high. This was discovered by injecting hisRNAP onto a 3% NTA surface that had not been exposed to nickel (data not shown). In this situation, the histidine tag should not have preference to bind to the NTA-group. Increasing amounts of hisRNAP were injected into the fluid cell while imaging. Three injections of 10 ng, then 20 and 100 ng, of hisRNAP were made at 5-min intervals. Single protein molecules were observed binding to the NTA groups ~4 min after injection of the 20-ng dose. Five min after injecting the 100 ng dose all NTA groups had nonspecifically bound hisRNAP and additional hisRNAP aggregated around the single hisRNAP molecules, which acted as nucleation sites for the aggregation. This aggregation phenomenon was also observed on nickel-charged 10% NTA-thiol surfaces after injection of large amounts (100 ng) of hisRNAP into the fluid cell (data not shown). These experiments suggest that there can be nonspecific interactions between the hisRNAP and the NTA groups. For these reasons the experiments to study the activity of the RNAP were carried out on 3% and 5% NTA surfaces, and the surfaces were loaded with amounts of RNAP below 10 ng.

The activity of the hisRNAP was assessed by imaging complexes of RNAP with a 42 base single-stranded circular DNA template (rolling circle), which produces huge RNA transcripts. Rolling circle complexes were specifically bound to a 5% NTA surface and imaged under continuously flowing buffer. After a buffer containing 5 μM NTPs was flowed through the fluid cell for 10 to 20 min the sample was removed, rinsed in excess water, dried in a stream of compressed air, imaged using tapping mode in air, and filamentous structures such as those in Fig. 6 were observed. These are similar in structure to those previously observed on mica surfaces (Kasas et al., 1997) and indicate that some of the hisRNAP molecules are active on these functionalized surfaces. Fig. 6 shows six representative images from these experiments. It is apparent that the activity or extent of transcription of hisRNAP molecules on these surfaces can vary substantially. Fig. 6, *a–c* show areas in

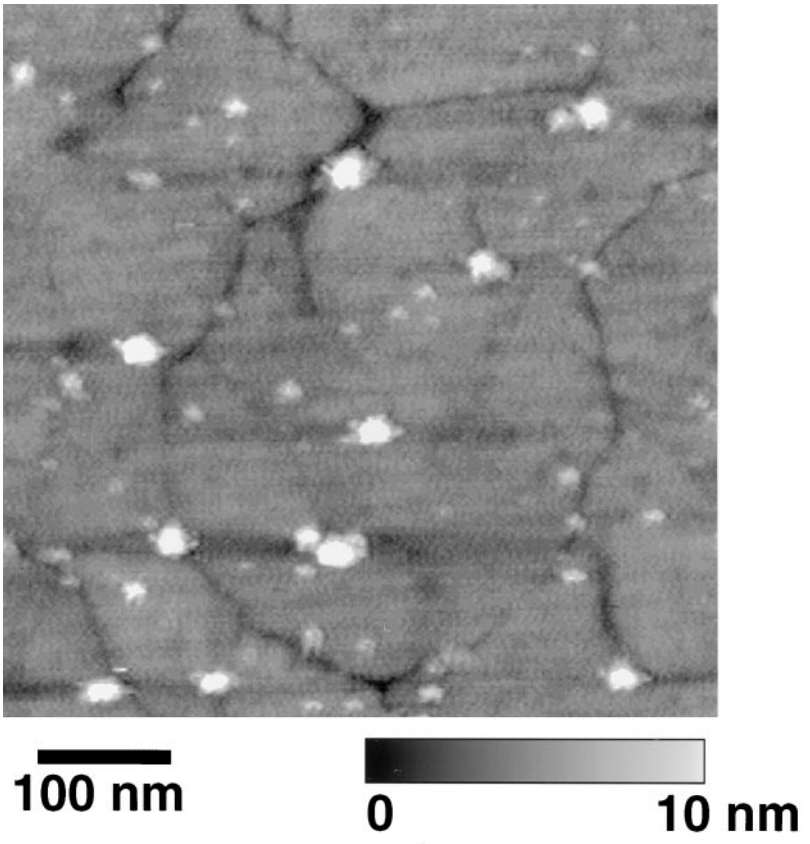

FIGURE 5 Representative AFM image of hisRNAP molecules specifically bound to nickel-NTA islands on the functionalized gold surface. The sample was prepared by incubating the protein with the surface outside the microscope. Ten individual hisRNAP molecules can be clearly visualized bound to the surface. The more abundant, smaller, lower features are NTA islands with no molecules bound. The underlying morphology of the gold can also be distinguished.

which there are hisRNAP still complexed with relatively small RNA transcripts (*large horizontal arrows*). Fig. 6, *d–f* show long filamentous RNA structures (outlined with *small arrows*) that have been produced. Also, fragmented pieces of RNA not associated with a hisRNAP can also be observed (see *diagonal arrows* in Fig. 6, *a* and *c*).

DISCUSSION

The template-stripped gold surfaces (Hegner et al., 1993) were ideal for these experiments because they were straightforward to prepare, could be stored until ready to be stripped, and were extremely flat over large areas (see Fig. 1). A combination of chemical and mechanical stripping was found to be most effective with our samples. The formation of the thiol monolayers is thought to have a self-cleaning effect on the gold surfaces, removing any unwanted absorbates (Martin Hegner, personal communication). When the relative concentration of the NTA-thiol is low (below 10%), the NTA forms elongated "islands" <100 nm in the maximum lateral dimension. A decrease in both the size and number of NTA islands on the surfaces was observed, as the fraction of NTA-thiol in the incubating solution was decreased from 10 to 3%. By keeping the concentration of NTA-thiol to 5% or below, the islands were small enough (10 to 20 nm across) to only allow the binding of single hisRNAP molecules to them (see Fig. 4). Below a critical concentration of hisRNAP of the order of 0.5 μg/ml, the hisRNAP always bound to the NTA islands above this concentration; in addition to binding to the islands, the hisRNAP flocculated around the islands or bound to grain boundaries in the gold structure, but never bound directly to the EG thiol.

On the gold surfaces covered with alkanethiols, depressions in the surface $\sim$1 nm in depth and 40 or 50 nm across were observed (see Fig. 2, *a* and *b*). These have a similar appearance to the "holes" that are known to be created through etching of the gold during the self-assembly process (McDermott et al., 1995; Schonenberger et al., 1994).

It is clear from these and previous studies (Hochuli et al., 1987; Kashlev et al., 1993; Sigal et al., 1996) of nickel-NTA (Ni-NTA)-his-protein binding that there is a specific interaction between the Ni-NTA group and the histidine tag. An open question is whether the hisRNAP interacts solely through the histidine tag or also has additional nonspecific interactions (e.g., hydrophobic). The hisRNAP in principle needs only one Ni-NTA group on the surface to bind to. The domains that we observed consist of many molecules. For instance, the "island" shown in Fig. 2 *c* is 20 nm $\times$ 70 nm. Assuming a tip broadening of 10 nm (tip radius of 5 nm) and a molecular separation of 0.5 nm (based on previous STM measurements on dodecanethiol; Schonenberger et al., 1994) it would give 2000 molecules in this domain. This is an upper estimate because the tip is unlikely to be sharper than the assumed value, and the packing of the NTA-thiol with a bulkier headgroup is unlikely to be so dense. To

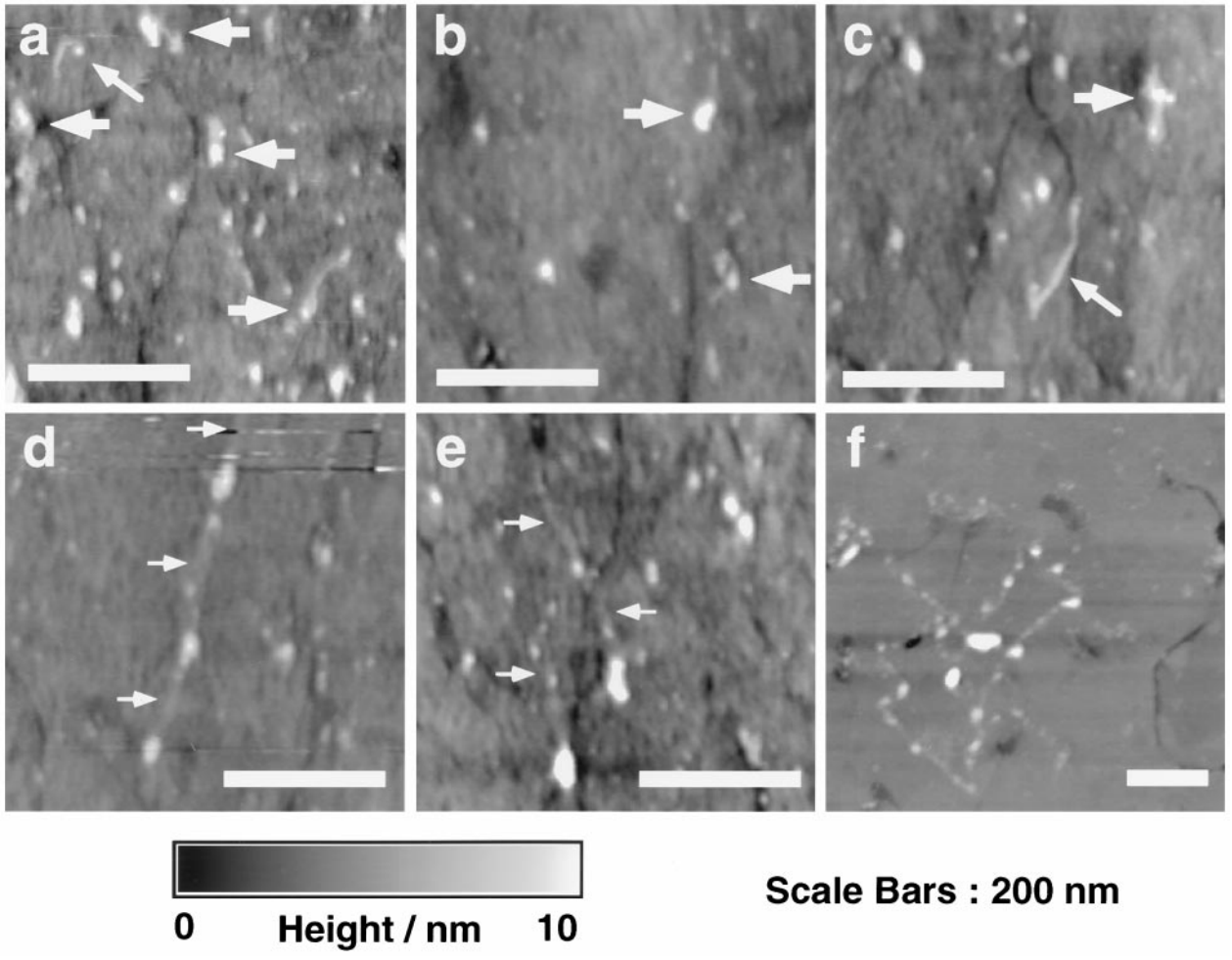

FIGURE 6 Tapping-mode AFM images taken in air of rolling complex samples specifically bound to the functionalized gold surfaces that were exposed to 5 μM NTPs in the microscope fluid cell for ~15 min. After this they were removed, rinsed in excess water, and dried for imaging in air. In Fig. 5, *a–c* hisRNAP complexed with small RNA transcripts can be observed (*large horizontal arrows*). In Fig. 5, *d–f*, longer filamentous RNA structures are seen (some marked with *small horizontal arrows*). Occasionally, fragments of RNA (*diagonal arrows* in *a* and *c*) are also observed. These structures are not observed on samples that have not been exposed to NTPs. The observation of the RNA strands confirms the activity of the hisRNAP on these surfaces. On air samples, the RNAP molecules can appear to have different sizes due to salt precipitation around them.

observe binding of single isolated hisRNAP molecules to the surface it was necessary to use 5% or less NTA-thiol in the incubating solution. The lowest amount of NTA-thiol we explored was 1%. Even for these islands of NTA we would expect maybe 200 molecules. With many NTA groups together it is likely that there are nonspecific interactions formed after the specific histidine interaction is established. Ideally, to achieve maximum activity of hisRNAP on the surface, it might be preferable to lower the content of NTA below 1%, say, to minimize unspecific interactions that might inhibit enzyme metabolism.

During the experiments to observe binding of the hisRNAP in situ, hisRNAP molecules would bind very soon after injection, within the time-scale of one to two images. Equilibrium conditions are assumed to have been reached when no more hisRNAP was observed binding or unbinding from the surface. In the experiment shown in Fig. 4 this was ~20–25 min after injection of the hisRNAP. It was clear that the tip also affected the binding in these in situ experiments. In Fig. 4 *b* one protein can be seen that takes a few frames to bind. In some experiments, binding of the hisRNAP was not observed within the initial scan, but on zooming out to a larger area hisRNAP molecules were observed already bound to the surface. The tip obviously affects the binding kinetics of the molecules to the surfaces, though it is not clear yet what might affect or prevent binding. It is conceivable that it depends upon the amount of energy per surface area that is imparted from the tip to the sample. If this is comparable to the binding energy of the protein to the surface, the tip may disrupt binding. The energy transfer from tip to sample depends on many factors, such as the scanning parameters (tapping amplitude and frequency, for instance), the surface properties and the cantilever dynamics.

The assay with the small single-stranded DNA circle (rolling circle) seems an attractive way to evaluate the

activity of individual hisRNAP molecules. Different hisRNAP molecules had transcripts of different lengths suggesting variations in activity from molecule to molecule, as previously observed in solution (Daubendiek et al., 1995) and on mica (Kasas et al., 1997). Quantifying the amount of RNA produced from a single molecule is rather difficult on these surfaces. Distinguishing the RNA transcripts from the background in the topographic images is not always easy on surfaces that are not atomically flat, and on dried samples having some traces of salt precipitated on them. It is almost certain that there is some salt associated with the RNA-protein complexes after drying, as evidenced by the variability of the RNAP sizes. Experience of imaging such complexes on mica (Kasas et al., 1997) makes us confident that the filamentous features are indeed RNA. These transcripts could not be imaged under the buffers we used, presumably because the RNA also has low affinity for the ethylene-glycol surface and was too mobile to be imaged.

CONCLUSIONS

We have created a general method for studying oriented proteins with AFM by combining a technique for making ultraflat gold (Hegner et al., 1993) with a system for binding histidine-tagged proteins to functionalized alkanethiolates (Sigal et al., 1996). The AFM showed that the NTA-thiol phase segregated from the EG-thiol into nanodomains that changed both in size and shape depending upon the relative concentrations of the two thiols in the incubating solution. Single histidine-tagged RNA polymerase (hisRNAP) (Kashlev et al., 1993) from *Escherichia coli* bacteria were observed binding to the NTA domains during imaging. The activity of these hisRNAP was demonstrated by using a small single-stranded circular DNA template (rolling circle) (Daubendiek et al., 1995) to produce large RNA transcripts that could be imaged in air but not under the buffers we used. The methods presented here enable single, active, specifically immobilized enzymes under physiological conditions to be imaged using AFM.

The authors thank Martin Hegner for advice on preparing template stripped gold surfaces, and Digital Instruments for AFM support. We acknowledge Roger Proksch for the design of the injection port for introduction of extremely small volumes into the AFM fluid cell.

This work was supported by NSF Grants DMR 9622169 and DMR 96-32716 from the Materials Research Laboratory and the Army Research Office, DAAHO4-96-1-0443. N.A. was funded by the Swedish Research Council for Engineering Sciences Grant 282-96-63.

REFERENCES

Akama, Y., E. Nishimura, A. Sakai, and H. Murakami. 1990. New scanning tunneling microscopy tip for measuring surface topography. *J. Vac. Sci. Technol. A.* 8:429–433.

Binnig, G., C. F. Quate, and C. Gerber. 1986. Atomic force microscope. *Phys. Rev. Lett.* 56:930.

Chidsey, C. E. D., D. N. Loiacono, T. Sleator, and S. Nakahara. 1988. STM study of the surface morphology of gold on mica. *Surf. Sci.* 200:45–66.

Cleveland, J. P., S. Manne, D. Bocek, and P. K. Hansma. 1993. A nondestructive method for determining the spring constant of cantilevers for scanning force microscopy. *Rev. Sci. Instrum.* 64:403–405.

Daubendiek, S. L., K. Ryan, and E. T. Kool. 1995. Rolling-circle RNA synthesis: circular oligonucleotides as efficient substrates for T7 RNA polymerase. *J. Am. Chem. Soc.* 117:7818–7819.

Delamarche, E., G. Sundarababu, H. Biebuyck, B. Michel, Ch. Gerber, H. Sigrist, H. Wolf, H. Ringsdorf, N. Xanthopoulos, and H. J. Mathieu. 1996. Immobilization of antibodies on a photoactive self-assembled monolayer on gold. *Langmuir.* 12:1997–2006.

Dreier, M., D. Anselmetti, T. Richmond, U. Dammer, and H.-J. Guntherodt. 1994. Dynamic force microscopy in liquids. *J. Appl. Phys.* 76:5095–5098.

Droz, E., M. Taborelli, P. Descouts, T. N. C. Wells, and R. C. Werlen. 1996. Covalent immobilization of immunoglobulins G and Fab′ fragments on gold substrates for scanning force microscopy imaging in liquids. *J. Vac. Sci. Technol. B.* 14:1422–1426.

Dubois, L. H., and R. G. Nuzzo. 1992. Synthesis, structure and properties of model organic surfaces. *Annu. Rev. Phys. Chem.* 43:437–463.

Florin, E.-L., V. T. Moy, and H. E. Gaub. 1994. Adhesion forces between individual ligand-receptor pairs. *Science.* 264:415–417.

Fritz, M., M. Radmacher, J. P. Cleveland, M. W. Allersma, R. J. Stewart, R. Gieselmann, P. Janmey, C. F. Schmidt, and P. K. Hansma. 1995. Imaging globular and filamentous proteins in physiological buffer solutions with tapping mode atomic force microscopy. *Langmuir.* 11: 3529–3535.

Hansma, P. K., J. P. Cleveland, M. Radmacher, D. A. Walters, P. Hillner, M. Bezanilla, M. Fritz, D. Vie, H. G. Hansma, C. B. Prater, J. Massie, L. Fukunaga, J. Gurley, and V. Elings. 1994. Tapping mode atomic force microscopy in liquids. *Appl. Phys. Lett.* 64:1738–1740.

Hegner, M., P. Wagner, and G. Semenza. 1993. Ultralarge atomically flat template-stripped Au surfaces for scanning probe microscopy. *Surf. Sci.* 291:39–46.

Hochuli, E., H. Dobeli, and A. Schacher. 1987. New metal chelate adsorbent selective for proteins and peptides containing neighboring histidine residues. *J. Chromatogr.* 411:177–184.

Kasas, S., N. H. Thomson, B. L. Smith, H. G. Hansma, X. Zhu, M. Guthold, C. Bustmante, E. T. Kool, M. Kashlev, and P. K. Hansma. 1997. *Escherichia coli* RNA polymerase activity observed using atomic force microscopy. *Biochemistry.* 36:461–468.

Kashlev, M., E. Martin, A. Polyakov, K. Severinov, V. Nikiforov, and A. Goldfarb. 1993. Histidine-tagged RNA polymerase: dissection of the transcription cycle using immobilized enzyme. *Gene.* 130:9–14.

Keller, D. J., and C. Chih-Chung. 1992. Imaging steep, high structures by scanning force microscopy with electron-beam deposited tips. *Surf. Sci.* 268:333–339.

Lee, G. U., L. A. Chrisey, and R. J. Colton. 1994a. Direct measurement of the forces between complementary strands of DNA. *Science.* 266: 771–773.

Lee, G. U., D. A. Kidwell, and R. J. Colton. 1994b. Sensing discrete streptavidin biotin interactions with the atomic force microscope. *Langmuir.* 10:354–357.

Manne, S., H.-J. Butt, S. A. C. Gould, and P. K. Hansma. 1990. Imaging metal atoms in air and water using the atomic force microscope. *Appl. Phys. Lett.* 56:1758–1759.

McDermott, C. A., M. T. McDermott, J.-B. Green, and M. D. Porter. 1995. Structural origins of the surface depressions at alkanethiolate monolayers on Au(111): a scanning tunneling and atomic force microscopic investigation. *J. Phys. Chem.* 99:13257–13267.

Moy, V. T., E. L. Florin, and H. E. Gaub. 1994. Intermolecular forces and energies between ligands and receptors. *Science.* 266:257–259.

Pale-Grosdemange, C., E. S. Simon, K. L. Prime, and G. M. Whitesides. 1991. Formation of self-assembled monolayers by chemisorption of derivatives of oligo(ethylene glycol) of structure $HS(CH_2)11(OCH_2CH_2)_mOH$ on gold. *J. Am. Chem. Soc.* 113:12–20.

Patel, N., M. C. Davies, M. Hartshorne, R. J. Heaton, C. J. Roberts, S. J. B. Tendler, and P. M. Williams. 1997. Immobilization of protein molecules

onto homogeneous and mixed carboxylate-terminated self-assembled monolayers. *Langmuir*. 13:6485–6490.

Putman, C. A. J., K. O. Vanderwerf, B. G. DeGrooth, N. F. Vanhulst, and J. Greve. 1994. Tapping-mode atomic force microscopy in liquid. *Appl. Phys. Lett.* 64:2454–2456.

Putnam, A., B. L. Blackford, M. H. Jericho, and M. O. Watanabe. 1989. Surface topography study of gold deposited on mica using scanning tunneling microscopy: effect of mica temperature. *Surf. Sci.* 217: 276–288.

Radmacher, M., M. Fritz, H. G. Hansma, and P. K. Hansma. 1994. Observation of enzyme activity with the atomic force microscope. *Science.* 265:1577–1579.

Rubin, E., S. Rumney IV, S. Wang, and E. T. Kool. 1995. Convergent DNA synthesis: a nonenzymatic dimerization approach to circular oligodeoxynucleotides. *Nucleic Acids Res.* 23:3547–3553.

Schonenberger, C., J. A. M. Sondag-Huethorst, J. Jorritsma, and L. G. J. Fokkink. 1994. What are the "holes" in self-assembled monolayers of alkanethiols on gold? *Langmuir*. 10:611–614.

Sigal, G. B., C. Bamdad, A. Barberis, J. Strominger, and G. M. Whitesides. 1996. A self-assembled monolayer for the binding and surface of histidine-tagged proteins by surface plasmon resonance. *Anal. Chem.* 68: 490–497.

Thomson, N. H., M. Fritz, M. Radmacher, J. P. Cleveland, C. Schmidt, and P. K. Hansma. 1996a. Protein tracking and detection of protein motion using atomic force microscopy. *Biophys. J.* 70:2421–2431.

Thomson, N. H., S. Kasas, B. Smith, H. G. Hansma, and P. K. Hansma. 1996b. Reversible binding of DNA to mica for AFM imaging. *Langmuir*. 12:5905.

Thomson, N. H., M. J. Miles, S. G. Ring, P. R. Shewry, and A. S. Tatham. 1994. Real-time imaging of enzymatic degradation of starch granules by atomic force microscopy. *J. Vac. Sci. Technol. B.* 12:1565.

Vancea, J., G. Reiss, F. Schneider, K. Bauer, and H. Hoffman. 1989. Substrate effects on the surface topography of evaporated gold films—a scanning tunnelling microscopy investigation. *Surf. Sci.* 218:108–126.

Wagner, P., P. Kernen, M. Hegner, E. Ungewickell, and G. Semenza. 1994. Covalent anchoring of proteins onto gold-directed NHS-terminated self-assembled monolayers in aqueous buffers: SFM images of clathrin cages and triskelia. *FEBS Lett.* 356:267–271.

Wagner, P., M. Hegner, P. Kernen, F. Zaugg, and G. Semenza. 1996. Covalent immobilization of native biomolecules onto Au(111) via N-hydroxysuccinimide ester functionalized self-assembled monolayers for scanning probe microscopy. *Biophys. J.* 70:2052–2066.

Whitesides, G. M., and C. G. Gorman. 1995. *In* Handbook of Surface Imaging and Visualization. CRC Press, Boca Raton, FL. 713–733.